Glaucoma

Variation of Laminar Depth in Normal Eyes With Age and Race

Lindsay A. Rhodes,[1] Carrie Huisingh,[1] John Johnstone,[2] Massimo Fazio,[1] Brandon Smith,[1] Mark Clark,[1] J. Crawford Downs,[1] Cynthia Owsley,[1] Michael J. A. Girard,[3,4] Jean Martial Mari,[5] and Christopher Girkin[1]

[1]Department of Ophthalmology, School of Medicine, University of Alabama at Birmingham, Birmingham, Alabama, United States
[2]Department of Computer and Information Sciences, College of Arts and Sciences, University of Alabama at Birmingham, Birmingham, Alabama, United States
[3]In Vivo Biomechanics Laboratory, Department of Biomedical Engineering, National University of Singapore, Singapore
[4]Singapore Eye Research Institute, Singapore National Eye Centre, Singapore
[5]Department of Medical Physics and Bioengineering, University College London, London, United Kingdom

PURPOSE. To determine if laminar depth (LD) and prelaminar tissue volume (PTV) are associated with age and race in healthy human eyes.

METHODS. Optic nerve head images from enhanced depth imaging spectral-domain optical coherence tomography of 166 normal eyes from 84 subjects of African descent (AD) and European descent (ED) were manually delineated to identify the principal surfaces: internal limiting membrane, Bruch's membrane (BM), anterior sclera (AS), and anterior surface of the lamina cribrosa. These four surfaces defined the LD and PTV using Bruch's membrane opening (BMO) and AS for reference structures. Generalized estimating equations were used to evaluate whether the effect of age on each outcome was differential by race.

RESULTS. When age was analyzed as a continuous variable, the interaction term between age and race was statistically significant for mean LD_{BMO} ($P = 0.015$) and mean LD_{AS} ($P = 0.0062$) after adjusting for axial length and BMO area. For every 1-year increase in age, the LD_{AS} was greater on average by 1.78 μm in AD subjects and less by 1.71 μm in ED subjects. Mean PTV was lower in the older subjects (1248×10^6 μm³ AD, 881×10^6 μm³ ED) compared to the younger subjects (1316×10^6 μm³ AD, 1102×10^6 μm³ ED) in both groups.

CONCLUSIONS. With increasing age, the LD changes differently across racial groups in normal subjects. The LD in ED subjects showed a significantly decreasing slope suggesting that the lamina moves anteriorly with age in this group.

Keywords: lamina cribrosa, laminar depth, spectral-domain optical coherence tomography

Individuals of African descent (AD) have a higher prevalence of primary open-angle glaucoma with worse visual outcomes from the disease compared to those of European descent (ED).[1–5] Investigation into the many possible causes of this disparity reveals racial and ethnic differences in the anatomy of the optic nerve head (ONH).[3,6–14] Variation in ONH parameters, such as larger optic discs, deeper cups, and thicker overall retinal nerve fiber layer thicknesses in AD individuals,[3,6,7,14–17] has been described using several different imaging modalities,[9,10,12,14,17–25] including scanning laser polarimetry,[18,19] confocal scanning laser ophthalmoscopy,[9,10,12,14,20–23] and time-domain[14,17,20,24] and spectral-domain optical coherence tomography (SDOCT).[24,25] In addition, normal aging of the optic nerve results in thinning of the retinal nerve fiber layer and neuroretinal rim with advancing age.[26–28]

Recent advances in SDOCT have allowed detailed visualization and measurement of deep ONH structures important in glaucomatous optic neuropathy: laminar position or depth (LD) and prelaminar tissue volume (PTV).[29–37] Several prior publications have reported laminar changes with glaucoma,[30,38–41] but no prior research has explored the relationship between age and laminar position across racial groups. Further, research

has been conducted using Bruch's membrane opening (BMO) as a reference plane, which has been shown to shift with age due to age-related thinning of the peripapillary choroid.[42–44]

Given that the lamina cribrosa (LC) is a critical load-bearing structure of the ONH, variations in laminar position with age and race may have important implications in the disparity of development and progression of glaucomatous optic neuropathy between AD and ED individuals. Understanding the variation in deep ONH structures, particularly in normal eyes, is necessary in order to effectively use these deep structural parameters for glaucoma detection and progression. The purpose of this study was to determine if LD and PTV are associated with age and across racial strata in healthy human eyes.

METHODS

The SDOCT data for this study were obtained from participants in two National Institutes of Health–funded cohort studies conducted at the University of Alabama at Birmingham: the African Descent and Glaucoma Evaluation Study (ADAGES)[45]
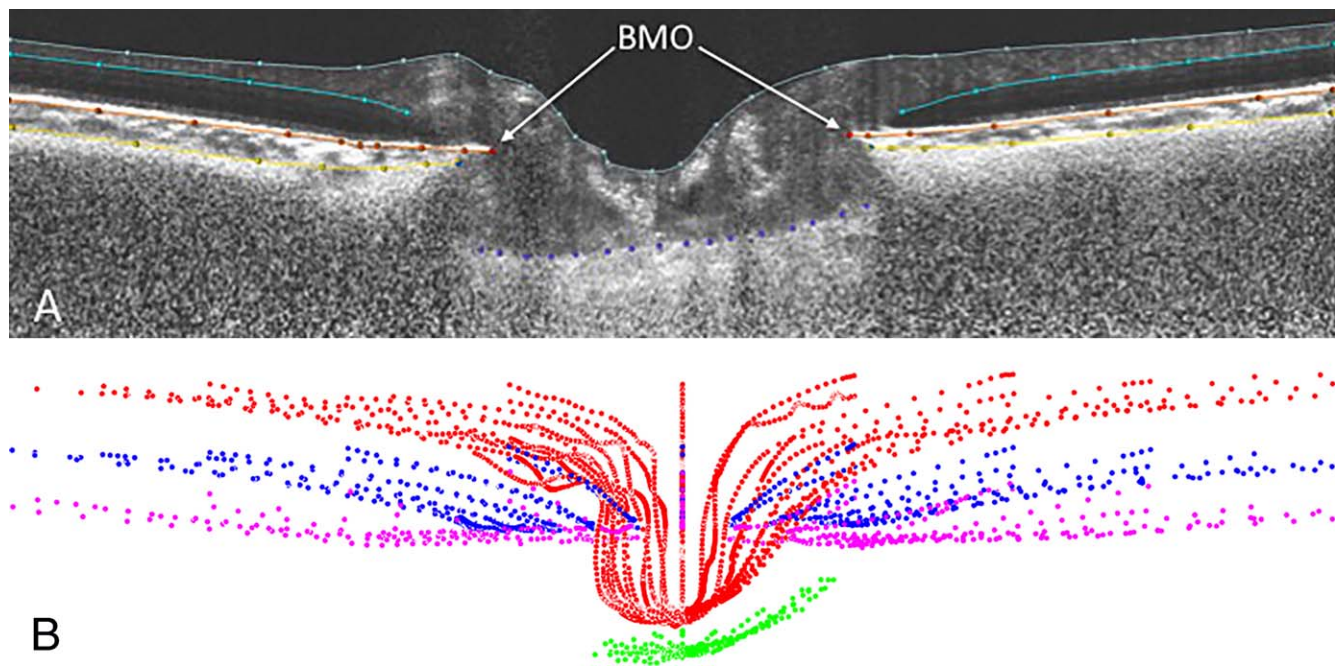
Investigative Ophthalmology & Visual Science

FIGURE 1. (A) Principal optic nerve head surfaces delineated: internal limiting membrane (*gray*), Bruch's membrane (*orange*), anterior sclera (*yellow*), and anterior surface of the lamina cribrosa (*purple*) within a sample SDOCT radial section. (B) Visualization of complete delineated surfaces: internal limiting membrane (*red*), Bruch's membrane (*blue*), anterior sclera (*magenta*), and anterior surface of the lamina cribrosa (*green*).

and the Alabama Study on Early Age-Related Macular Degeneration (ALSTAR).[46] ADAGES enrolled individuals of both AD and ED, while ALSTAR enrolled primarily subjects of ED (95% of the subjects). Only subjects without evidence of ocular diseases that would affect the optic nerve, retina, or choroid were included, as defined below. The imaging methodologies followed in ADAGES and ALSTAR were identical. All participants from each study gave written informed consent. The University of Alabama at Birmingham institutional review board approved the study methods, and these methods adhered to the tenets of the Declaration of Helsinki. Healthy subjects for both studies were recruited to join the study by advertisement and from primary eye care clinics.

Each participant underwent a complete ophthalmological exam that included medical history, Snellen best-corrected visual acuity, Early Treatment Diabetic Retinopathy Study (ETDRS) visual acuity, color vision, slit-lamp biomicroscopy, applanation tonometry for intraocular pressure (IOP), central corneal thickness measurement (ADAGES only), axial length measurement (ADAGES only), dilated funduscopy, stereoscopic ophthalmoscopy of the optic disc, and stereoscopic fundus photography. Standard Swedish Interactive Thresholding Algorithm 24-2 perimetry was performed to define normality for inclusion in this study (see below).

Inclusion/Exclusion Criteria

Participants were older than 18 years of age for the ADAGES study and ≥ 60 years for the ALSTAR study. Eligible participants had open iridocorneal angles, a best-corrected acuity of 20/40 or better, and refractive error ≤ 5.0 diopters sphere and 3.0 diopters cylinder. Patients with diabetes and any retinal, corneal, or optic nerve disease were excluded. A family history of glaucoma was allowed. Participants were excluded if they had a history of intraocular surgery (except for uncomplicated cataract surgery), elevated IOP (>22 mm Hg) at the time of the study, a history of elevated IOP, prior use of glaucoma medication, other intraocular eye disease, or other diseases

affecting visual field (e.g., pituitary lesions, demyelinating diseases, human immunodeficiency virus positive or acquired immune deficiency syndrome). Further, patients were excluded if there was a diagnosis of Alzheimer's disease, Parkinson's disease, or previous brain injury including stroke, psychoses, or other neurological or psychiatric conditions that would prevent participation in a psychophysical test.

We required a reliable test on 24-2 standard automated perimetry (Carl Zeiss Meditec, Dublin, CA, USA) using the Swedish Interactive Thresholding Algorithm in both eyes at baseline for inclusion in the study. Reliability was defined as <33% false positives, false negatives, and fixation losses. A field was considered normal if the pattern standard deviation was not triggered at 5% or less, the Glaucoma Hemifield Test was within normal limits, and the field showed no sign of glaucomatous defect based on subjective evaluation from the enrolling clinician. The optic nerves were assessed by stereoscopic photos by a fellowship-trained glaucoma specialist. Subjects with any structural finding suggestive of glaucoma (i.e., notching, rim thinning, disc hemorrhages, or retinal nerve fiber layer defects as judged) were excluded.

SDOCT Image Acquisition, Processing, and Quantification

All subjects underwent SDOCT imaging with the Spectralis OCT (Family Acquisition Module 5.4.8.0; Heidelberg Engineering, Heidelberg, Germany) with forty-eight 20° radial scans centered on the ONH using the enhanced depth imaging (EDI) mode.[30] Scans were evaluated for image quality by the operator, and images were reacquired if there was improper B-scan positioning, a quality score < 20, or poor centration of the ONH. A total of 168 volume scans from both eyes of 84 study subjects were included. Radial scans were acquired using a scan-averaging setting of 9 ($n = 108$; ADAGES) or 12 ($n = 60$; ALSTAR). All other characteristics of the imaging protocols were identical.
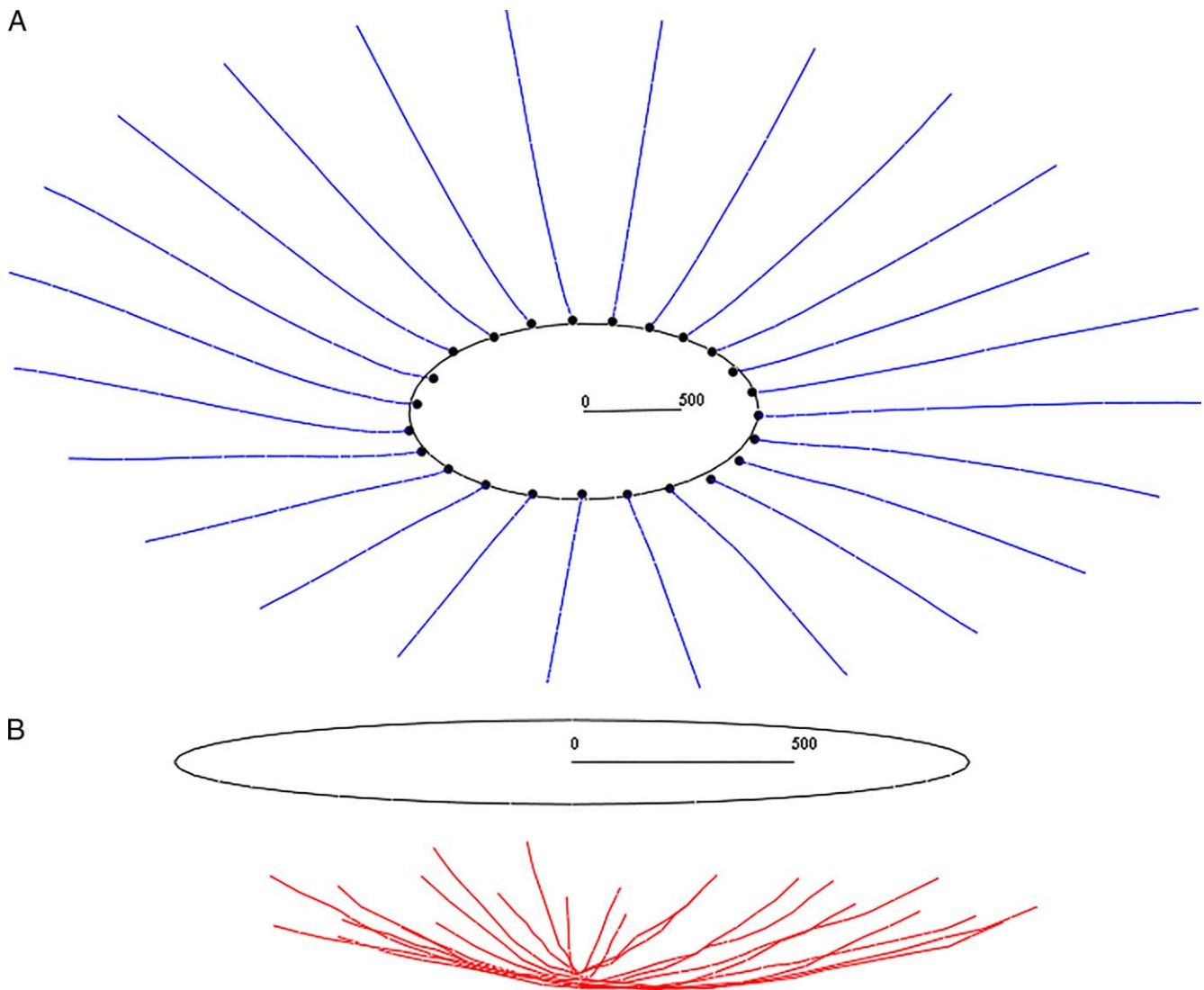
A

B

FIGURE 2. (A) The Bruch reference structure: Bruch's membrane (*blue*), Bruch's membrane opening (BMO) point cloud (*black dots*), and BMO ellipse (*black ellipse*, which lies in the BMO plane). A 500-μm measure is included to illustrate scale. (B) Computing laminar depth (LC). The lamina cribrosa (*red*) and BMO ellipse (*black*) are shown. The BMO ellipse lies in the BMO plane. LD_{BMO} is the distance from this plane. A 500-μm measure is included for scale.

In order to enhance the visibility of the deeper tissue, all B-scans from all SDOCT volumes were postprocessed using adaptive light attenuation compensation with contrast and threshold exponents of 2.[47,48] This algorithm has been demonstrated to (1) significantly increase the interlayer contrast (a measure of tissue boundary visibility) across all major ONH tissue boundaries; (2) significantly reduce the intralayer contrast (a measure of blood vessel shadow visibility) within all tissues; (3) improve the visibility of LC insertions and focal laminar defects in some cases; and (4) remove noise overamplification in the deepest tissue layers. Two eyes were eliminated due to inadequate visualization of the anterior sclera (AS) following compensation. Adaptive compensation allowed visualization and delineation of characteristic structures such as Bruch's membrane (BM) and the anterior surface of the LC.

Radial SDOCT scan volumes were loaded and aligned in custom software based on the Visualization Toolkit (VTK, Clifton Park, NY, USA) that was developed for three-dimensional delineation of histologic and OCT data as described in prior publications.[29,49] For each eye, a trained observer masked to subject characteristics manually delineated 24 equally spaced radial sections. Principal surfaces delineated included retinal surface based on internal limiting membrane (ILM), BM, AS, and anterior surface of the LC (Figs. 1A, 1B). These four surfaces were used for all further analysis in this study to define the LD and PTV as described below. An average of 3313 manually delineated points (range, 2171–5486) was used to define the four surfaces (ILM, BM, AS, LC); an average of 202 points (range, 23–534) was used to define the anterior laminar surface.

Computing LD. The measurements of LD were developed from a laminar surface constructed from manually delineated points as previously described.[36,49–51] Laminar depth must be measured against a stable reference structure. Since prior work[44] has demonstrated significant posterior migration of BMO principally caused by choroidal thinning with age, this study employed two reference structures: one based on BMO and another based on AS. Laminar depth measures the distance of the LC from a reference plane, either a BMO plane (LD_{BMO}) or a scleral plane (LD_{AS}). The definition and computation of mean LD require the definition of a reference structure against which to measure depth, a surface reconstruction and
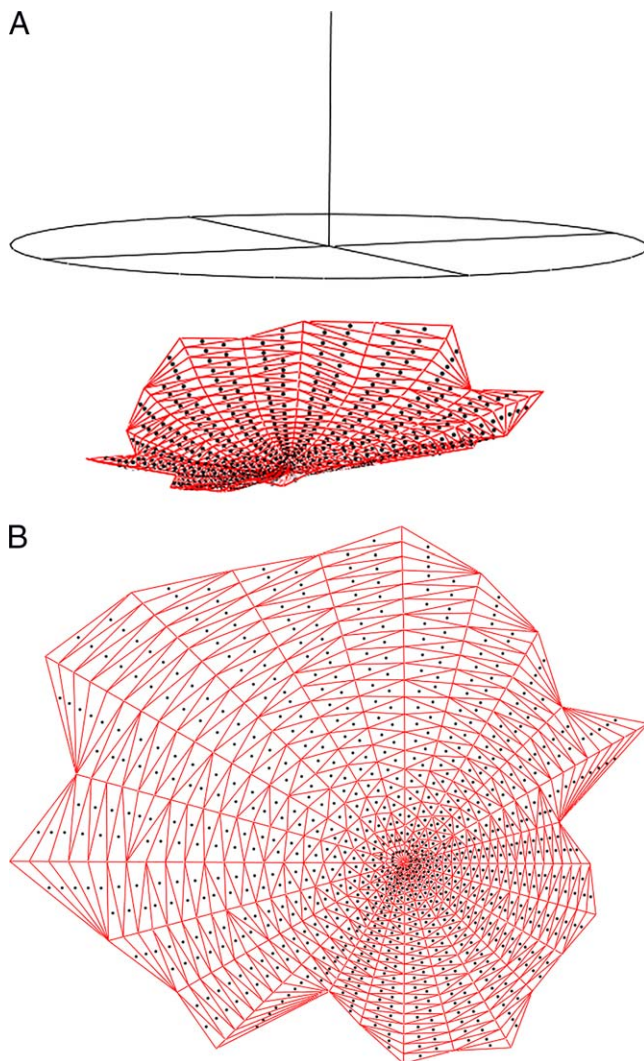
A

B

FIGURE 3. (**A**) The laminar surface used for sampling of laminar depth (LD) across the lamina. This is a reconstruction of the delineated (visible) portion of the lamina by a triangle mesh, as bounded by the BMO ellipse in *black* above the *red* mesh. Laminar depth is sampled at the centroids of these triangles (marked by *black dots*). This nonuniform sampling of LD is weighted by triangle area to simulate a uniform sampling of LD. (**B**) Enlarged three-dimensional reconstruction of the laminar surface.

sampling for mean depth, and the use of a suitable coordinate frame for the manually delineated point clouds. We consider each of these issues in turn.

A natural reference structure for ONH morphometry is based on BM (Figs. 2A, 2B). Since BMO is the anterior opening of the neural canal and is nearly planar and nearly elliptical, its best-fitting plane (BMO plane) and ellipse (BMO ellipse) reflect its shape well and define a useful reference structure for depth. The BMO plane and ellipse (which is used below to define both the Bruch frame and scleral reference structure) are computed by principal component analysis.[52] The distance of an LC point from the BMO plane is its LD with respect to BMO (LD_{BMO}). Note that care must be taken in computing the center of the BMO ellipse, which is not the sample mean of the points delineating the BMO, as the center axis of the delineation planes is not coincident with the center axis of the BMO elliptic cylinder.

The computation of mean LD_{BMO} requires the computation of depth over a uniform sampling of a surface reconstruction of the raw delineated data. In preparation for the surface reconstruction, the LC sections are resampled. Each LC section is downsampled (to remove oversampling that interferes with interpolation) using a variant of the Douglas-Peucker curve simplification algorithm,[53] interpolated by a cubic B-spline curve,[54] uniformly resampled to define a robust sampling for surface construction, and clipped by the BMO elliptic cylinder. An optimal triangle surface mesh (one of minimal surface area) is built from these resampled LC sections.[55]

A uniform sampling of depth across this surface is approximated by the weighting of a nonuniform sampling, using area as the weight. Laminar depth is measured at the triangle centroids, and weighted by the area of the triangle. In particular, if $\{T_i\}_i \in_I$ are the triangles of the LC mesh, C_i is the centroid of T_i, and A is the total area of the LC mesh, mean LD is

$$mean\ LD = \sum_{i \varepsilon I} \frac{area(Ti)}{A} *LD(Ci). \qquad (1)$$

Many algorithms for uniform sampling of the LC surface were considered, and this yielded the best results. Note that the density of the mesh, and thus the sampling, may be controlled through the density of the uniform sampling of the sections. The computation of LD_{BMO} was limited to those points within the BMO elliptic cylinder. In contrast to sampling just a few select points, this approach robustly samples across a reconstruction of the entire laminar surface built from the compensated three-dimensional SDOCT dataset (Figs. 3A, 3B).

The computation of LD_{BMO} may be simplified by working in a special coordinate frame: A Bruch frame is a coordinate frame whose origin is the center of the BMO ellipse, $z = 0$ plane is the BMO plane, and $z > 0$ half-space is the laminar half-space of the BMO plane. In a Bruch frame, the LD of a point is its z-coordinate.

In summary, an algorithm for the computation of LD_{BMO} is as follows. The Bruch structure (BMO plane, BMO ellipse, laminar half-space) is computed and the LC moved to a Bruch frame. The LC sections are uniformly resampled; an optimal mesh is built from these LC sections; and mean LD_{BMO} is computed as a weighted average of the mesh centroid depths.

Depth may also be computed relative to a scleral reference structure. Since the anterior boundary of the AS cannot be found reliably in all images, a direct analogue to the Bruch structure is not used. Instead, the scleral structure is built using an interior disk-like region (the region of the AS between 1700 and 1800 μm from the axis of the BMO cylinder, the right elliptic cylinder defined by the BMO ellipse, orthogonal to the BMO plane). Like the BMO, this region is almost planar. The scleral representative of an AS half-section (Fig. 4) is the mean of the samples that lie between 1700 and 1800 μm from the axis of the BMO cylinder (using Euclidean, not geodesic distance). The mean is used (as opposed to the point at 1750 μm, e.g.) as a smoothing operation. The scleral plane (ellipse) is the best-fitting plane (ellipse) of the point cloud of scleral representatives, analogous to the BMO plane/ellipse. Replacing the BMO plane by the scleral plane, we have LD based on a scleral reference plane (distance of LC from scleral plane, LD_{AS}). These measurements are again simplified by using a special frame, where depth becomes z-coordinate.

Computing PTV. The PTV is the volume bounded by the ILM on the anterior side, the LC on the posterior side, and the BMO cylinder. Construction of the PTV requires extrapolation of the LC to the BMO cylinder, construction of a hexahedral mesh of the volume, and computation of the volume of this mesh. We consider each of these issues in turn.
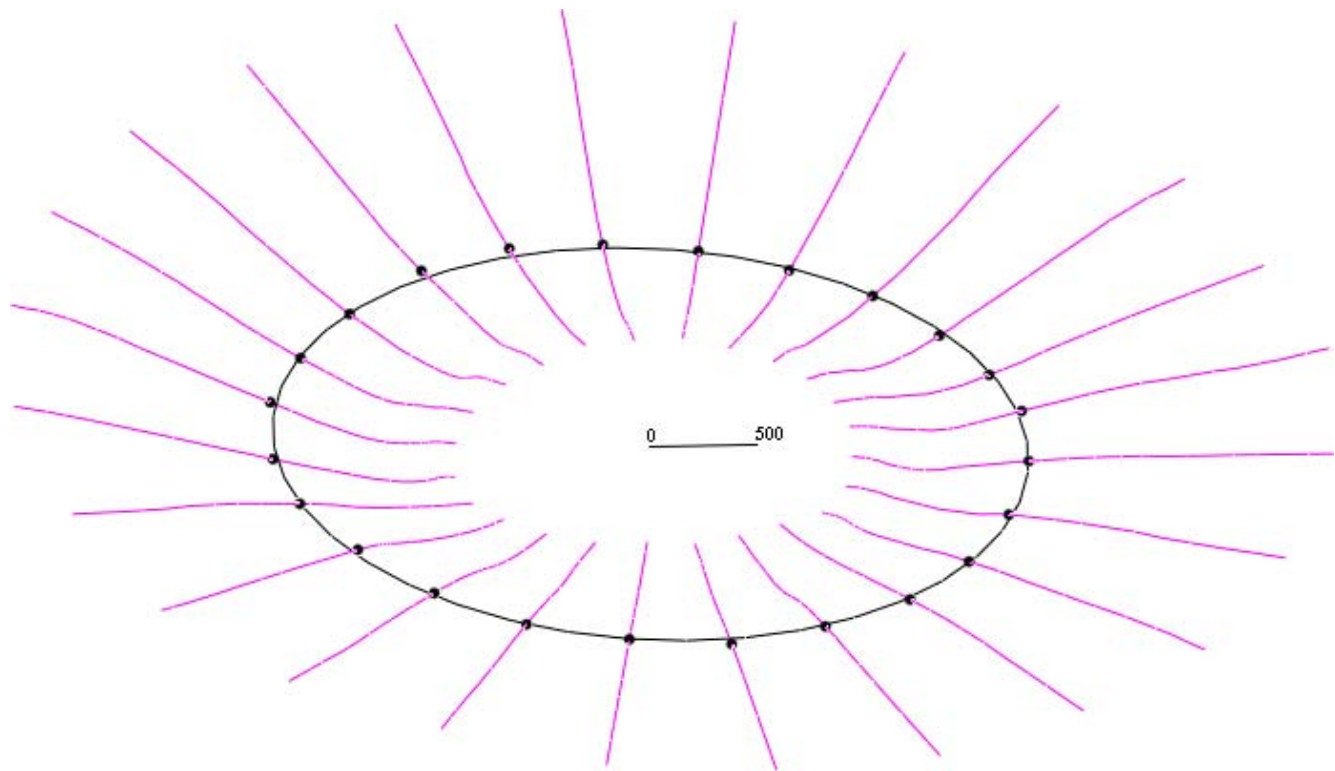
FIGURE 4. The scleral reference structure: anterior sclera (*magenta*), scleral representatives located at 1700 to 1800 µm from the axis of the BMO cylinder (*black dots*), and scleral ellipse (*black ellipse*, which lies in the scleral plane). LD_{AS} is the distance from this plane to the lamina. A 500-µm measure is included to illustrate scale.

Before building the hexahedral mesh of the volume, the LC is extrapolated to the BMO cylinder to close the volume (Figs. 5A, 5B). The LC sections are extrapolated by best-fitting lines of local neighborhoods at either end of the section. Extrapolation by a parabola was also attempted and rejected. Before extrapolation, particularly short sections are culled, since they are unreliable for extrapolation (30% coverage of the BMO cylinder radius on both sides of the axis of rotation was required in these datasets). After extrapolation, missing half-sections are filled in by interpolation from neighboring half-sections. Datasets with too much missing data are rejected (33 of the 166 datasets). Although this extrapolation is not anatomically accurate, it is at least consistent across datasets.

The PTV is computed through the construction of a hexahedral mesh, a partition of the volume into hexahedra (Figs. 6a, 6b). The interior of the PTV cannot be meshed using standard meshing software (e.g., TetGen, Stellar, or TetMesh)[56] since these packages require a watertight boundary, and the ILM/LC surfaces are not watertight (due to noise in the delineations). Each hexahedron (a generalization of the cube with six faces and eight vertices) or hex of the hexahedral mesh is built by firing four rays (a ray quartet) at the ILM, at the LC, and at the BMO cylinder and recording their intersections. In the typical case, each ray hits the ILM and LC once before it hits the BMO cylinder, yielding a hex defined by four points on the ILM and four points on the LC; but there are several other cases, including degenerate pentahedra, hexes involving the BMO cylinder, and ray quartets that define more than one hex. The ray quartets are chosen using a series of spokes (Fig. 6c): A spoke is a directed ray starting at the axis of rotation, orthogonal to the axis of rotation, and lying in one of the imaging planes. The spokes are sampled uniformly, and the four rays of a quartet are fired from spoke samples i and $i+1$ of spokes j and $j+1$, along rays parallel to the axis of rotation.

Once a hex mesh is constructed, its volume is the sum of its hex volumes. We use the tetrakis decomposition of a hex into 24 tetrahedra,[57] which reduces the volume of a hex to the volume of a tetrahedron.

Computing Choroidal Thickness. Choroidal thickness was defined as the distance between BM and AS, measured along a normal ray to BM. Since BM exhibits local irregularities yet each section of BM is pseudolinear, it is more robust to replace each section of BM by a line for the purposes of computing the normal of BM. This thickness is sampled along BM between 1000 and 1500 µm away from BMO, and the mean of these thicknesses is used as the overall choroidal thickness. This location was chosen because the AS surface is difficult to visualize (and thus to define accurately) in regions more adjacent to the border of the neural canal, due to shadowing from the retinal vessels and reduced signal intensity from thick overlying tissues.

Statistical Analysis

Optic nerve characteristics are presented by age group (young < 65 years; old ≥ 65 years) and race (AD and ED) for descriptive purposes. Generalized estimating equations (GEE) were used to evaluate whether the effect of age on each outcome was differential by race, with the ED group as the reference group. The generalized estimating equation allows the model to account for the within-subject correlation among fellow eyes from the same individual. Models were adjusted for the potentially confounding effects of axial length and BMO area (a surrogate for optic disc size). Age, axial length, and BMO area were continuous variables in the adjusted model. Separate models were used for the dependent variables, LD_{BMO}, LD_{AS}, and PTV. P values less than 0.05 were considered statistically significant.
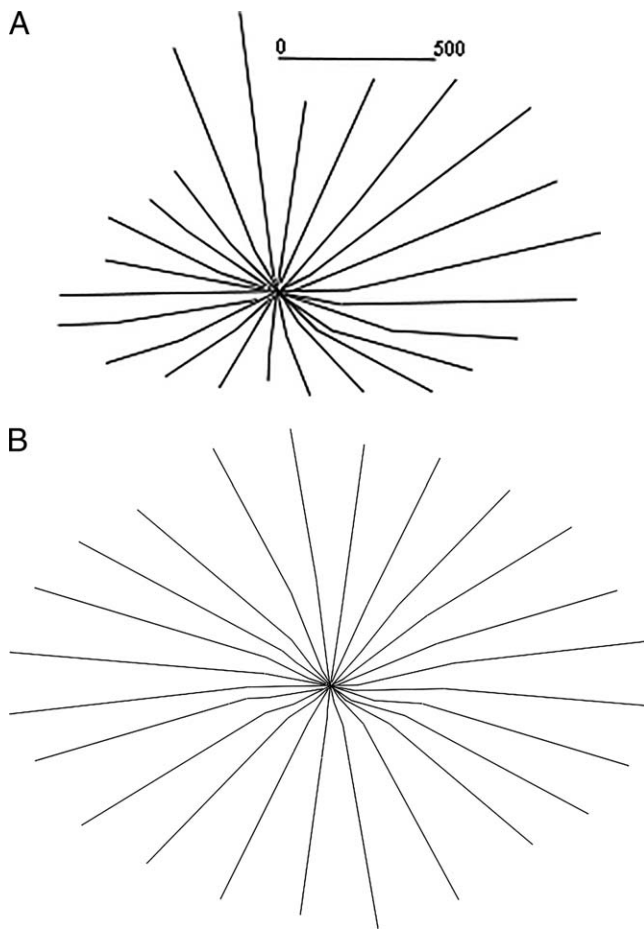
A

B

FIGURE 5. Extrapolation. (**A**) Original delineation of lamina cribrosa and (**B**) its extrapolation, well beyond the BMO cylinder. A 500-μm measure in (**A**) illustrates scale.

RESULTS

The final study sample consisted of 166 eyes from 84 subjects. Sixty percent of the subjects were ED and the remaining were AD. Subjects ranged in age from 29 to 92 years with a mean age of 58 years (Table 1); however, those in the AD group were significantly younger (mean 50.4 years, SD 11.3) than those in

TABLE 1. Demographic and Ocular Characteristics of the Study Population ($N = 166$)

Variable	N (%) or Mean (SD)
Age, y	58.4 (15.5)
Race	
African descent	64 (39%)
European descent	102 (61%)
Sex	
Female	120 (72%)
Male	46 (28%)
Axial length,* mm	23.7 (1.0)
BMO area, $\times 10^6$ μm²	1.9 (0.4)

* 12 missing data ($N = 154$).

the ED group (mean 63.4 years, SD 15.6) ($P < 0.0001$). Approximately three-quarters (72%) were female. The average axial length in all subjects was 23.7 mm (SD 1.0), and BMO area was 1.9×10^6 μm² (SD 0.4).

Table 2 compares mean optic nerve characteristics stratified by age group and race. Mean LD_{BMO} was less among both the older AD and ED subjects compared to the younger subjects. Mean LD_{AS} was greater among older AD subjects (354 vs. 334 μm) compared to younger subjects ($P = 0.49$), and slightly less among older than younger ED subjects (309 vs. 316 μm) ($P = 0.75$) (Fig. 7A). As expected, the mean PTV was lower in the older age group (1248×10^6 μm³ AD, 881×10^6 μm³ ED) compared to the younger age group (1316×10^6 μm³ AD, 1101×10^6 μm³ ED) in both groups ($P = 0.60$ for AD; $P = 0.0006$ for ED) (Fig. 7B).

The broad categories of age in Table 2 may result in an imperfect adjustment of the sample. When age was analyzed as a continuous variable, the interaction term between age and race was statistically significant in the models for mean LD_{AS} ($P = 0.0062$) and mean LD_{BMO} ($P = 0.015$) after adjusting for axial length and BMO area (Table 3). This shows that the linear relationship between age and each outcome was differential by race. As shown in Figure 8, for every 1-year increase in age, the LD_{AS} was greater on average by 1.78 μm in the AD subjects and less by 1.71 μm in the ED subjects. Among ED subjects, the slope between age and LD_{AS} was significantly different from zero ($P = 0.018$, age term), but not among AD subjects ($P =$
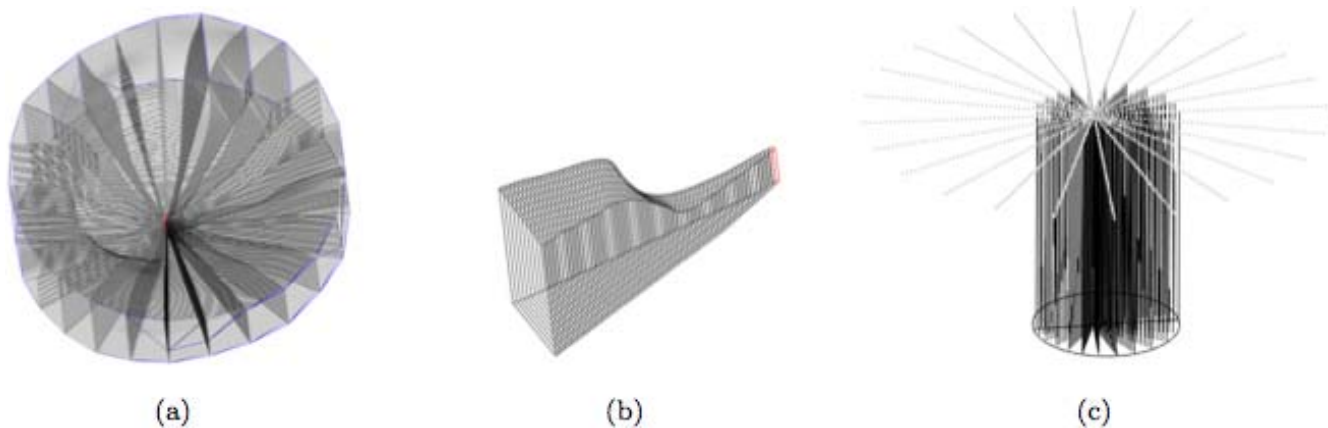

FIGURE 6. (**a**) Hexahedral mesh of the prelaminar tissue volume. (**b**) A slice of the hexahedral mesh between two half-sections. (**c**) The spokes (*top*) used to build a hexahedral mesh, and some of the rays (*vertical lines*) fired at the internal limiting membrane, lamina cribrosa, and Bruch's membrane opening (BMO) cylinder (a finer sampling is actually used). The BMO ellipse is also shown (at *bottom*).
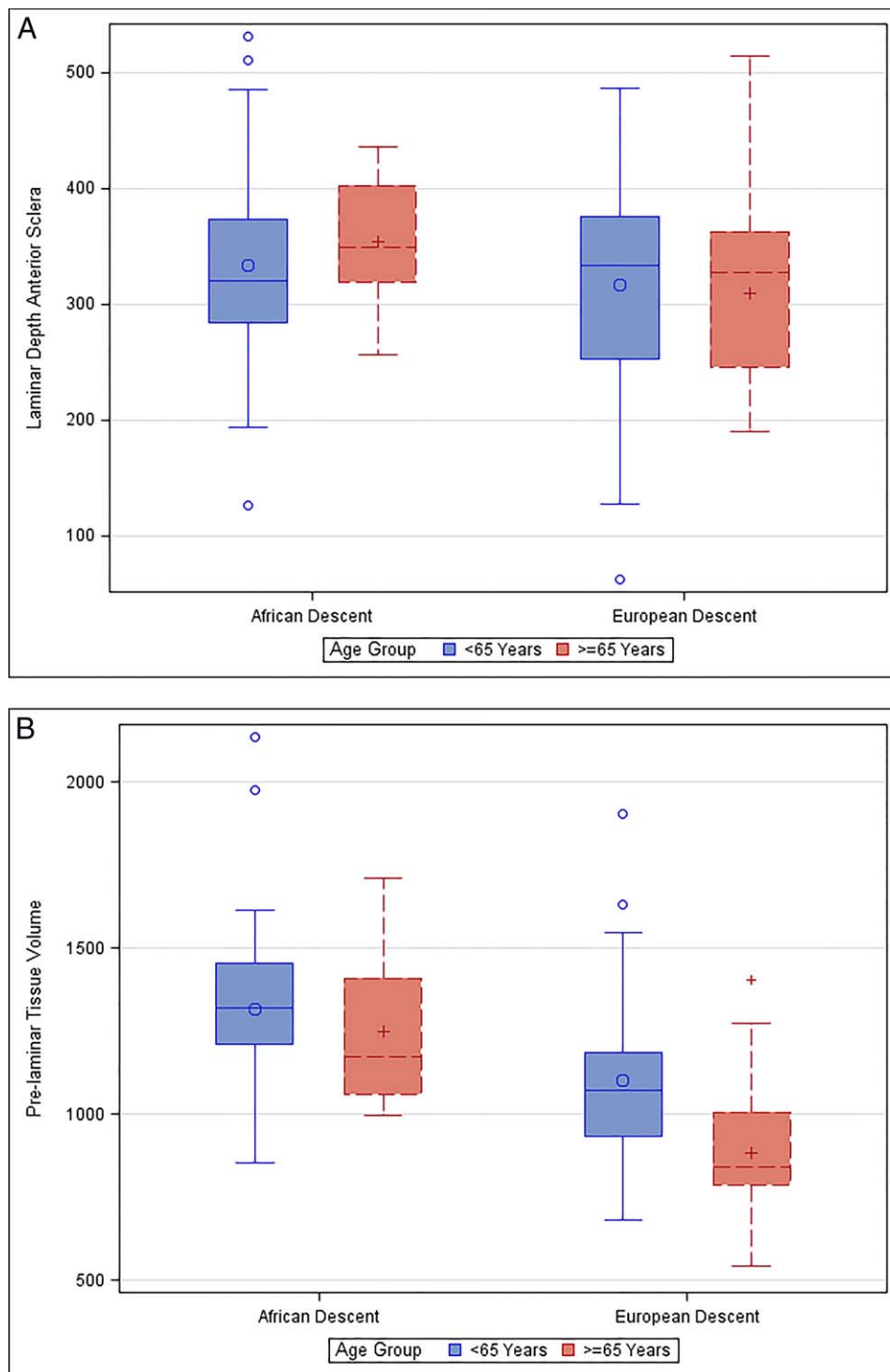
FIGURE 7. (**A**) Laminar depth in the scleral reference plane in micrometers, grouped by race (African and European descent) and age (<65 and >65 years) ($P = 0.49$ for AD, $P = 0.75$ for ED). (**B**) Prelaminar tissue volume (in 10^6 μm^3) grouped by race (African and European descent) and age (<65 and >65 years) ($P = 0.60$ for AD; $P = 0.0006$ for ED).

0.091, age term). For LD_{BMO}, every 1-year increase in age was associated with a decrease in LD by 0.08 μm in AD subjects as compared to a decrease of 2.84 μm in ED subjects. Among ED subjects, the slope between age and LD_{BMO} was significantly different from zero ($P < 0.0001$, age term), but not among AD subjects when the AD group was used as the referent category ($P = 0.93$, age term). The analysis was repeated excluding ED participants over age 78 so that the AD and ED groups had comparable age ranges; the pattern of results was unchanged (LD_{AS} $P = 0.038$, LD_{BMO} $P = 0.0052$). The age and race interaction term was not statistically significant in the model for PTV ($P = 0.62$), suggesting that a lower PTV with increasing age was similar between those in the AD and ED groups (Table 4).

TABLE 2. Optic Nerve Characteristics by Race and Age Group ($N = 166$ Eyes)

	Young, <65 Y; African Descent, N = 56		Old, ≥65 Y; African Descent, N = 8		Young, <65 Y; European Descent, N = 54		Old, ≥65 Y; European Descent, N = 48	
	Mean	SD	Mean	SD	Mean	SD	Mean	SD
Choroidal thickness, μm	205.96	47.09	135.88	48.05	166.17	44.80	119.87	40.50
LD_{BMO}, μm	413.88	75.06	365.38	64.48	382.43	93.29	337.73	82.41
LD_{AS}, μm	333.61	83.84	353.75	60.32	316.39	87.60	309.20	78.69
PTV, $\times 10^6$ μm³	1316.49	239.63	1248.41	263.21	1102.64	233.55	880.94	200.28

TABLE 3. Age and Race Effects on Laminar Depth Relative to Both the Bruch's Membrane (LD_{BMO}) and Scleral (LD_{AS}) Reference Planes, Including the Age-Race Interaction, as Estimated by Generalized Estimating Equation Regression Analysis

|	LD_{BMO}				LD_{AS}			
Independent Variable	Coefficient	SE	z Value	P Value	Coefficient	SE	z Value	P Value
Intercept	704.74	208.87	3.37	0.0007	743.78	199.57	3.73	0.0002
Age	−2.84	0.71	−3.98	<0.0001	−1.71	0.72	−2.36	0.018
Race	−111.22	65.12	−1.71	0.088	−162.75	72.28	−2.25	0.024
Age-race interaction	2.76	1.13	2.44	0.015	3.49	1.28	2.74	0.0062
Axial length	−3.30	8.53	−0.39	0.70	−11.39	7.87	−1.45	0.15
BMO area	−48.85	18.70	−2.61	0.0090	−30.84	21.012	−1.47	0.14
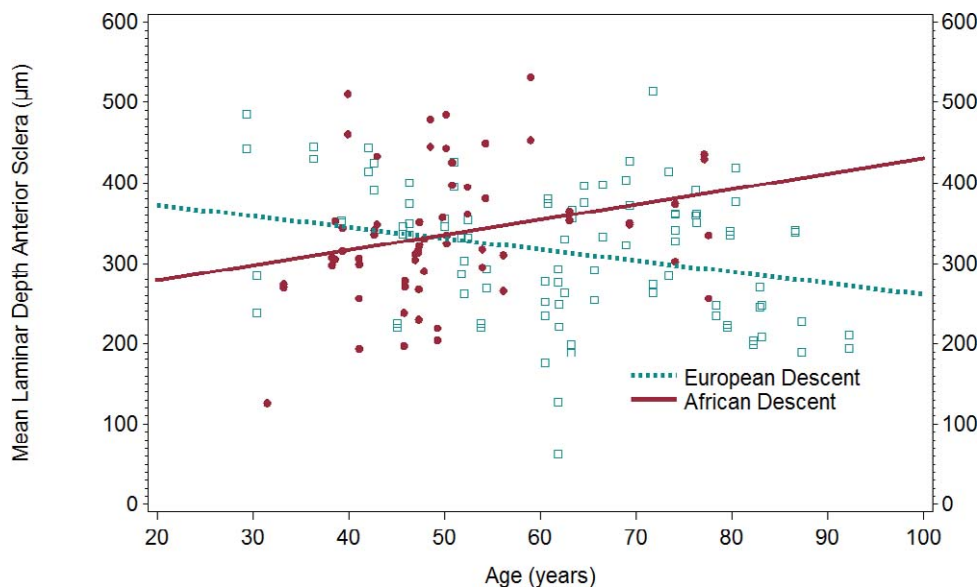
FIGURE 8. Scatterplot and regression line of age and mean LD_{AS} by race. LD_{AS}, laminar depth anterior sclera.

TABLE 4. Age and Race Effects on Prelaminar Tissue Volume, Including the Age-Race Interaction, as Estimated by Generalized Estimating Equation Regression Analysis

Independent Variable	Coefficient	SE	z Value	P Value
Intercept	1028.075	376.85	2.73	0.0064
Age	−5.23	2.34	−2.24	0.025
Race	166.28	198.77	0.84	0.40
Age-race interaction	−1.78	3.60	−0.49	0.62
Axial length	−19.17	17.40	−1.10	0.27
BMO area	435.75	57.098	7.63	<0.0001

DISCUSSION

Understanding the variation in LC position and PTV in normal eyes is important, as these are visualized structures in the ONH that are relevant to the development and progression of glaucomatous optic neuropathy. To the best of our knowledge, this is the first study to use SDOCT to examine the variation in deep ONH structures with both age and race. Our results suggest that with increasing age, laminar position changes differentially by race in normal, nonglaucomatous AD versus ED subjects when using both the anterior scleral surface and BMO as reference points. Using a scleral reference point, the

LD_{AS} in ED subjects showed a decreasing slope that was statistically different from zero, suggesting that the lamina becomes shallower (more anterior) with age in people of ED relative to the AS reference point. The AD group had a positive slope (i.e., deepening of the LC with age) that was not statistically different from a slope of zero; however, it was significantly different from the slope of the ED group, suggesting that the laminar position is either stable or may be in a more posterior position with age, relative to the AS reference point. When BMO was used as the reference point for LD, ED subjects also showed a decreasing slope (more anterior LC with age) that was statistically different from zero; however, the LD in the AD group had a negative slope that was not statistically different from a slope of zero. Lastly, PTV was lower with increasing age in both AD and ED groups, indicating a progressive loss of prelaminar optic nerve tissue with age.

While the reduction in LD with age when using BMO as a reference plane (LD_{BMO}) is likely due to the posterior migration of BMO, as previously demonstrated,[44] the smaller but significant anteriorization of the LC relative to the scleral-based reference plane (LD_{AS}) in the ED group is more difficult to interpret. Theoretically, shallowing of the LC is possible with age if there is remodeling in response to gradual expansion of the neural canal with age.[58] Anteriorization of the LC has been demonstrated following acute IOP elevation in primates[58–60] and humans[58]; and our results could represent the effects of chronic age-related remodeling of the sclera, neural canal wall, and/or the LC. Alternatively, this effect could be due to a shift in the scleral reference plane relative to the position of the lamina, perhaps due to posterior peripapillary bowing of the sclera. While this has not been observed, it would imply that there is currently no stable reference plane by which we can definitively quantify deep optic nerve structures. Hence, development of a progressive approach that examines changes in local image features would be optimal for detecting changes in deep optic nerve structures with age and with the onset and progression of glaucoma. In any case, the aging effects of the load-bearing tissues of the ONH visualized by SDOCT clearly differ between racial groups, but whether this represents posterior migration of the LC in AD individuals or anteriorization of the LC in ED individuals would need to be confirmed with a feature-based approach.

The decrease in PTV with age in both racial groups likely represents progressive loss of prelaminar tissue, consisting of retinal nerve fibers and supporting elements such as astrocytes and capillaries. Several prior studies have demonstrated a decrease in retinal nerve fiber layer thickness with increasing age in normal eyes using in vivo imaging studies.[17,28,61] Prelaminar tissue loss has been demonstrated with SDOCT in experimental glaucoma.[62]

There are limited previous studies using in vivo EDI SDOCT to measure LD. Lee et al.[38] analyzed 137 Korean glaucoma patients and found a mean laminar cup depth of 560 μm. In the manual delineation of the LC and its depth, blood vessel shadowing obscured the nasal aspect of the lamina and prevented measurement in this region. Furlanetto et al.[39] evaluated the LD of glaucomatous eyes and compared them to normal eyes, finding a statistically significant variation in mean depth of 438 μm in the glaucoma group compared to 353 μm in the normal group. That study was based on 11 horizontal B-scans per optic nerve and included predominantly ED patients with no AD subjects. Recently, Seo et al.[63] measured the anterior LC depth of 300 normal eyes in Korea, finding an average depth of 402 μm. In that study, age did not impact LD, although an association was found between sex and axial length.

The previous studies used BM and BMO plane as a reference for measuring mean LD. However, previous work has clearly demonstrated that BMO moves posteriorly with age due to decreasing choroidal thickness, thereby confounding LD measurements with age-related changes in peripapillary choroidal thickness.[42–44] The current study found an overall shallower mean LD based on a scleral reference when compared to previous studies in normal eyes that used BMO as a reference. The mean LD_{BMO} in our study was similar to those of previous studies. The current study explores laminar position in greater detail using a robust sampling method with three-dimensional manual delineation of an average of 3133 points in the ONH and 202 points in the anterior lamina, combined with LC surface reconstruction. The previously mentioned studies determined LD based on between 11 and 30 points.[38,39,63] Lastly, previous studies have not examined the association between race and LD, particularly comparing people of AD and ED. Our study is also the first to quantify PTV using EDI SDOCT.

This study has several limitations. First, the study is a cross-sectional evaluation of age, race, and LD. Additional research with a longitudinal study is needed to evaluate rates of change of laminar position and PTV with age and race. While the racial groups differ in age, a similar pattern was seen in age-adjusted models even when excluding the older participants in the ED group, so this is unlikely to have impacted our results. The sample size was relatively small, but similarly to the previous studies reviewed above, allowed observation of statistically significant variations of the investigated parameters. We can conclude that the lamina becomes significantly shallower respective to the scleral surface in the ED group, and that in the AD group, the lamina deepens in association with age compared to what occurs in the ED group. However, the study may be underpowered to detect laminar deepening with age in the AD group.

In conclusion, this study describes the variation in LD and PTV using EDI SDOCT in normal eyes, finding that LD and PTV have an association with advancing age. While PTV changes are not associated with race, the lamina cribrosa was significantly more anterior with increasing age in persons of ED in contrast to the individuals of AD.

Acknowledgments

Disclosure: **L.A. Rhodes**, None; **C. Huisingh**, None; **J. Johnstone**, None; **M. Fazio**, None; **B. Smith**, None; **M. Clark**, None; **J.C. Downs**, None; **C. Owsley**, None; **M.J.A. Girard**, None; **J.M. Mari**, None; **C. Girkin**, None

References

1. Sommer A, Tielsch JM, Katz J, et al. Racial differences in the cause-specific prevalence of blindness in east Baltimore. *N Engl J Med*. 1991;325:1412–1417.

2. Tielsch JM, Sommer A, Katz J, Royall RM, Quigley HA, Javitt J. Racial variations in the prevalence of primary open-angle glaucoma. The Baltimore Eye Survey. *JAMA*. 1991;266:369–374.

3. Varma R, Tielsch JM, Quigley HA, et al. Race-, age-, gender-, and refractive error-related differences in the normal optic disc. *Arch Ophthalmol*. 1994;112:1068–1076.

4. Sommer A. Glaucoma risk factors observed in the Baltimore Eye Survey. *Curr Opin Ophthalmol*. 1996;7:93–98.

5. Hoffmann EM, Zangwill LM, Crowston JG, Weinreb RN. Optic disk size and glaucoma. *Surv Ophthalmol*. 2007;52:32–49.

6. Beck RW, Messner DK, Musch DC, Martonyi CL, Lichter PR. Is there a racial difference in physiologic cup size? *Ophthalmology*. 1985;92:873–876.

7. Chi T, Ritch R, Stickler D, Pitman B, Tsai C, Hsieh FY. Racial differences in optic nerve head parameters. *Arch Ophthalmol*. 1989;107:836–839.

8. Tsai CS, Zangwill L, Gonzalez C, et al. Ethnic differences in optic nerve head topography. *J Glaucoma*. 1995;4:248–257.

9. Girkin CA, McGwin G Jr, McNeal SF, DeLeon-Ortega J. Racial differences in the association between optic disc topography and early glaucoma. *Invest Ophthalmol Vis Sci*. 2003;44:3382–3387.

10. Girkin CA, McGwin G Jr, Long C, DeLeon-Ortega J, Graf CM, Everett AW. Subjective and objective optic nerve assessment in African Americans and whites. *Invest Ophthalmol Vis Sci*. 2004;45:2272–2278.

11. Zangwill LM, Weinreb RN, Berry CC, et al. The confocal scanning laser ophthalmoscopy ancillary study to the ocular hypertension treatment study: study design and baseline factors. *Am J Ophthalmol*. 2004;137:219–227.

12. Girkin CA, McGwin G Jr, Xie A, Deleon-Ortega J. Differences in optic disc topography between black and white normal subjects. *Ophthalmology*. 2005;112:33–39.

13. Girkin CA, DeLeon-Ortega JE, Xie A, McGwin G, Arthur SN, Monheit BE. Comparison of the Moorfields classification using confocal scanning laser ophthalmoscopy and subjective optic disc classification in detecting glaucoma in blacks and whites. *Ophthalmology*. 2006;113:2144–2149.

14. Girkin CA, Sample PA, Liebmann JM, et al. African Descent and Glaucoma Evaluation Study (ADAGES): II. Ancestry differences in optic disc, retinal nerve fiber layer, and macular structure in healthy subjects. *Arch Ophthalmol*. 2010;128:541–550.

15. Dandona L, Quigley HA, Brown AE, Enger C. Quantitative regional structure of the normal human lamina cribrosa. A racial comparison. *Arch Ophthalmol*. 1990;108:393–398.

16. Quigley HA, Brown AE, Morrison JD, Drance SM. The size and shape of the optic disc in normal human eyes. *Arch Ophthalmol*. 1990;108:51–57.

17. Budenz DL, Anderson DR, Varma R, et al. Determinants of normal retinal nerve fiber layer thickness measured by Stratus OCT. *Ophthalmology*. 2007;114:1046–1052.

18. Poinoosawmy D, Fontana L, Wu JX, Fitzke FW, Hitchings RA. Variation of nerve fibre layer thickness measurements with age and ethnicity by scanning laser polarimetry. *Br J Ophthalmol*. 1997;81:350–354.

19. Costa VP, Lauande-Pimentel R, Fonseca RA, Magacho L. The influence of age, sex, race, refractive error and optic disc parameters on the sensitivity and specificity of scanning laser polarimetry. *Acta Ophthalmol Scand*. 2004;82:419–425.

20. Racette L, Boden C, Kleinhandler SL, et al. Differences in visual function and optic nerve structure between healthy eyes of blacks and whites. *Arch Ophthalmol*. 2005;123:1547–1553.

21. Zelefsky JR, Harizman N, Mora R, et al. Assessment of a race-specific normative HRT-III database to differentiate glaucomatous from normal eyes. *J Glaucoma*. 2006;15:548–551.

22. De Leon-Ortega JE, Sakata LM, Monheit BE, McGwin G Jr, Arthur SN, Girkin CA. Comparison of diagnostic accuracy of Heidelberg Retina Tomograph II and Heidelberg Retina Tomograph 3 to discriminate glaucomatous and nonglaucomatous eyes. *Am J Ophthalmol*. 2007;144:525–532.

23. Seider MI, Lee RY, Wang D, Pekmezci M, Porco TC, Lin SC. Optic disk size variability between African, Asian, white, Hispanic, and Filipino Americans using Heidelberg retinal tomography. *J Glaucoma*. 2009;18:595–600.

24. Gonzalez-Garcia AO, Vizzeri G, Bowd C, Medeiros FA, Zangwill LM, Weinreb RN. Reproducibility of RTVue retinal nerve fiber layer thickness and optic disc measurements and agreement with Stratus optical coherence tomography measurements. *Am J Ophthalmol*. 2009;147:1067–1074, 1074.e1061.

25. Mwanza JC, Chang RT, Budenz DL, et al. Reproducibility of peripapillary retinal nerve fiber layer thickness and optic nerve head parameters measured with cirrus HD-OCT in glaucomatous eyes. *Invest Ophthalmol Vis Sci*. 2010;51:5724–5730.

26. Ford BA, Artes PH, McCormick TA, Nicolela MT, LeBlanc RP, Chauhan BC. Comparison of data analysis tools for detection of glaucoma with the Heidelberg Retina Tomograph. *Ophthalmology*. 2003;110:1145–1150.

27. Celebi AR, Mirza GE. Age-related change in retinal nerve fiber layer thickness measured with spectral domain optical coherence tomography. *Invest Ophthalmol Vis Sci*. 2013;54:8095–8103.

28. Leung CK, Yu M, Weinreb RN, et al. Retinal nerve fiber layer imaging with spectral-domain optical coherence tomography: a prospective analysis of age-related loss. *Ophthalmology*. 2012;119:731–737.

29. Strouthidis NG, Yang H, Downs JC, Burgoyne CF. Comparison of clinical and three-dimensional histomorphometric optic disc margin anatomy. *Invest Ophthalmol Vis Sci*. 2009;50:2165–2174.

30. Lee EJ, Kim TW, Weinreb RN, Park KH, Kim SH, Kim DM. Visualization of the lamina cribrosa using enhanced depth imaging spectral-domain optical coherence tomography. *Am J Ophthalmol*. 2011;152:87–95, e81.

31. Park HY, Jeon SH, Park CK. Enhanced depth imaging detects lamina cribrosa thickness differences in normal tension glaucoma and primary open-angle glaucoma. *Ophthalmology*. 2012;119:10–20.

32. Park SC, De Moraes CG, Teng CC, Tello C, Liebmann JM, Ritch R. Enhanced depth imaging optical coherence tomography of deep optic nerve complex structures in glaucoma. *Ophthalmology*. 2012;119:3–9.

33. Park SC, Kiumehr S, Teng CC, Tello C, Liebmann JM, Ritch R. Horizontal central ridge of the lamina cribrosa and regional differences in laminar insertion in healthy subjects. *Invest Ophthalmol Vis Sci*. 2012;53:1610–1616.

34. Reis AS, O'Leary N, Yang H, et al. Influence of clinically invisible, but optical coherence tomography detected, optic disc margin anatomy on neuroretinal rim evaluation. *Invest Ophthalmol Vis Sci*. 2012;53:1852–1860.

35. Reis AS, Sharpe GP, Yang H, Nicolela MT, Burgoyne CF, Chauhan BC. Optic disc margin anatomy in patients with glaucoma and normal controls with spectral domain optical coherence tomography. *Ophthalmology*. 2012;119:738–747.

36. Yang H, Qi J, Hardin C, et al. Spectral-domain optical coherence tomography enhanced depth imaging of the normal and glaucomatous nonhuman primate optic nerve head. *Invest Ophthalmol Vis Sci*. 2012;53:394–405.

37. You JY, Park SC, Su D, Teng CC, Liebmann JM, Ritch R. Focal lamina cribrosa defects associated with glaucomatous rim thinning and acquired pits. *JAMA Ophthalmol*. 2013;131:314–320.

38. Lee EJ, Kim TW, Weinreb RN, et al. Three-dimensional evaluation of the lamina cribrosa using spectral-domain optical coherence tomography in glaucoma. *Invest Ophthalmol Vis Sci*. 2012;53:198–204.

39. Furlanetto RL, Park SC, Damle UJ, et al. Posterior displacement of the lamina cribrosa in glaucoma: in vivo interindividual and intereye comparisons. *Invest Ophthalmol Vis Sci*. 2013;54:4836–4842.

40. Ren R, Yang H, Gardiner SK, et al. Anterior lamina cribrosa surface depth, age, and visual field sensitivity in the Portland

Progression Project. *Invest Ophthalmol Vis Sci*. 2014;55: 1531–1539.

41. Rho CR, Park HY, Lee NY, Park CK. Clock-hour laminar displacement and age in primary open-angle glaucoma and normal tension glaucoma. *Clin Experiment Ophthalmol*. 2012;40:e183–e189.

42. Barteselli G, Chhablani J, El-Emam S, et al. Choroidal volume variations with age, axial length, and sex in healthy subjects: a three-dimensional analysis. *Ophthalmology*. 2012;119:2572–2578.

43. Huang W, Wang W, Zhou M, et al. Peripapillary choroidal thickness in healthy Chinese subjects. *BMC Ophthalmol*. 2013;13:23.

44. Johnstone J, Fazio M, Rojananuangnit K, et al. Variation of the axial location of Bruch's membrane opening with age, choroidal thickness, and race. *Invest Ophthalmol Vis Sci*. 2014;55:2004–2009.

45. Sample PA, Girkin CA, Zangwill LM, et al. The African Descent and Glaucoma Evaluation Study (ADAGES): design and baseline data. *Arch Ophthalmol*. 2009;127:1136–1145.

46. Owsley C, Huisingh C, Jackson GR, et al. Associations between abnormal rod-mediated dark adaptation and health and functioning in older adults with normal macular health [published online ahead of print May 22, 2014]. *Invest Ophthalmol Vis Sci*. doi:10.1167/iovs.14-14502.

47. Girard MJ, Strouthidis N, Ethier CR, Mari JM. Shadow removal and contrast enhancement in optical coherence tomography images of the human optic nerve head. *Invest Ophthalmol Vis Sci*. 2011;52:7738–7748.

48. Mari JM, Strouthidis NG, Park SC, Girard MJ. Enhancement of lamina cribrosa visibility in optical coherence tomography images using adaptive compensation. *Invest Ophthalmol Vis Sci*. 2013;54:2238–2247.

49. Downs JC, Yang H, Girkin C, et al. Three-dimensional histomorphometry of the normal and early glaucomatous monkey optic nerve head: neural canal and subarachnoid space architecture. *Invest Ophthalmol Vis Sci*. 2007;48:3195–3208.

50. Fortune B, Yang H, Strouthidis NG, et al. The effect of acute intraocular pressure elevation on peripapillary retinal thickness, retinal nerve fiber layer thickness, and retardance. *Invest Ophthalmol Vis Sci*. 2009;50:4719–4726.

51. Strouthidis NG, Grimm J, Williams GA, Cull GA, Wilson DJ, Burgoyne CF. A comparison of optic nerve head morphology viewed by spectral domain optical coherence tomography and by serial histology. *Invest Ophthalmol Vis Sci*. 2010;51:1464–1474.

52. Duda R, Hart P, Stork D. *Pattern Classification*. New York: Wiley-Interscience; 2000.

53. Ballard D. *Computer Vision*. Englewood Cliffs, NJ: Prentice Hall; 1982.

54. Farin G. *Curves and Surfaces for Computer Aided Geometric Design*. New York: Academic Press; 1993.

55. Fuchs H, Kedem Z, Uselton S. Optimal surface reconstruction from planar contours. *Comm ACM*. 1977;20:693–702.

56. Sandia National Laboratories. CUBIT. Available at: acubit. sandia.gov. Accessed May 2014.

57. Grandy J. *Efficient Computation of Volume of Hexahedral Cells*. Report no. UCRL-ID-128886. Livermore, CA: Lawrence Livermore National Laboratory; 1997.

58. Agoumi Y, Sharpe GP, Hutchison DM, Nicolela MT, Artes PH, Chauhan BC. Laminar and prelaminar tissue displacement during intraocular pressure elevation in glaucoma patients and healthy controls. *Ophthalmology*. 2011;118:52–59.

59. Yang H, Downs JC, Sigal IA, Roberts MD, Thompson H, Burgoyne CF. Deformation of the normal monkey optic nerve head connective tissue after acute IOP elevation within 3-D histomorphometric reconstructions. *Invest Ophthalmol Vis Sci*. 2009;50:5785–5799.

60. Strouthidis NG, Fortune B, Yang H, Sigal IA, Burgoyne CF. Effect of acute intraocular pressure elevation on the monkey optic nerve head as detected by spectral domain optical coherence tomography. *Invest Ophthalmol Vis Sci*. 2011;52: 9431–9437.

61. Hirasawa H, Tomidokoro A, Araie M, et al. Peripapillary retinal nerve fiber layer thickness determined by spectral-domain optical coherence tomography in ophthalmologically normal eyes. *Arch Ophthalmol*. 2010;128:1420–1426.

62. Strouthidis NG, Fortune B, Yang H, Sigal IA, Burgoyne CF. Longitudinal change detected by spectral domain optical coherence tomography in the optic nerve head and peripapillary retina in experimental glaucoma. *Invest Ophthalmol Vis Sci*. 2011;52:1206–1219.

63. Seo JH, Kim TW, Weinreb RN. Lamina cribrosa depth in healthy eyes. *Invest Ophthalmol Vis Sci*. 2014;55:1241–1251.